International Journal of Mechanical, Industrial and Aerospace Sciences
ISSN: 2517-9950
Vol:9, No:9, 2015

Vibration Analysis of a Solar Powered UAV

Kevin Anderson, Sukhwinder Singh Sandhu, Nouh Anies, Shilpa Ravichandra, Steven Dobbs, Donald Edberg

***Abstract*—**This paper presents the results of a Finite Element based vibration analysis of a solar powered Unmanned Aerial Vehicle (UAV). The purpose of this paper was to quantify the free vibration, forced vibration response due to differing point inputs in order to predict the relative response magnitudes and frequencies at various wing locations of vibration induced power generators (magnet in coil) excited by gust and/or control surface pulse-decays used to help power the flight of the electric UAV. A Fluid Structure Interaction (FSI) study was performed in order to ascertain pertinent design stresses and deflections as well as aerodynamic parameters of the UAV airfoil. The 10 ft span airfoil is modeled using Mylar as the primary material. Results show that the free mode in bending is 4.8 Hz while the first forced bending mode is on range of 16.2 to 16.7 Hz depending on the location of excitation. The free torsional bending mode is 28.3 Hz, and the first forced torsional mode is range of 26.4 to 27.8 Hz, depending on the location of excitation. The FSI results predict the coefficients of aerodynamic drag and lift of 0.0052 and 0.077, respectively, which matches hand-calculations used to validate the Finite Element based results. FSI based maximum von Mises stresses and deflections were found to be 0.282 MPa and 3.4 mm, respectively. Dynamic pressures on the airfoil range from 1.04 to 1.23 kPa corresponding to velocity magnitudes in range of 22 to 66 m/s.

***Keywords*—**ANSYS, finite element, FSI, UAV, vibrations.

I. Introduction

THIS paper describes the vibration analysis and fluid-structure-interaction of an electric motor Unmanned Air Vehicle (UAV) with a 10 foot wing span used for investigating various schemes for hybrid power efficiency including solar cells and magnet in coil vibration response power generators that has been developed at Cal Poly Pomona's Aerospace Engineering Department. Applications for UAVs capable of extreme endurance and loitering times are becoming more important. An integration of multidisciplinary technologies including autonomous flight controls, UAV electric powered aircraft, solar cells and a new manufacturing approach for fabricating Graphene super capacitors that are significantly more efficient than current batteries are key for enabling 24/7 flight times.

The vibration generators can be positioned inside the wing at various locations to be excited by gusts and control surface pulses to produce structural vibrations to produce power to the aircraft storage devices. In order to aid the further design of the Cal Poly Pomona UAV a FEM based Vibration/FSI study was performed in order to: i) optimize the locations of the magnet in coil generators. Since the generators are a bit heavy they affect the frequencies and mode shapes of the wing.

The end goal is to find the wing span and cord locations where the vibration modes offer the highest response magnitudes to excite the vibration generators, ii) identify the wing frequencies so the magnet-spring-coil natural oscillation frequency can be tuned by selecting the springs stiffness that suspend the magnet to match the wing frequency. This tuning will be used to amplify the motion of the magnet oscillation due to a wing vibration, Results for drag, lift, von Mises stresses, and critical modes of vibration will presented. Results of the FSI used to design the solar powered aircraft will be summarized herein. The undergraduate multidisciplinary team and the UAV is shown in Fig. 1.

Fig. 1 Cal Poly Pomona solar powered UAV team

II. Literature Review

Recent years have seen an increased focus on the research and development of UAV system which can fly for a substantial period of time in order to realize specific missions. The work of [1] gives results of a flight test and power simulations of an UAV powered by solar cells, a fuel cell and batteries. The mid-class UAV system used in [1] consists of three types of power sources operating simultaneously. These power sources are designed and constructed to share the same operation voltage range and connect to the power bus without additional converters or controllers. The flight test of the target UAV system was conducted for 22.13 hours. In the area of solar powered UAVs the pioneering mission of solar UAV flight is outlined in [2]. The details of a 48 hour mission of a solar powered UAV are given in [3]. Power limitations are the current bottleneck of solar / battery powered UAVs. The work of [4] presents Sizing and Preliminary Hardware Testing of Solar Powered UAV. The study of [5] gives an overview of a custom battery pack used to power a UAV. The work of [6] addresses Automatic Battery Replacement System for UAVs:

K. R. Anderson is with the Non-linear FEA/CFD Multiphysics Simulation Laboratory in the Mechanical Engineering Department, California State Polytechnic University, Pomona, CA 91768 USA (1-909-869-2687; Fax: 1-909-869-4341; e-mail: kranderson1@cpp.edu).

S. Singh, N. Anies and S. Ravichandra are with the Mechanical Engineering Department, California State Polytechnic University, Pomona, CA 91768 USA.

S. K. Dobbs and D. Edberg are with the Aerospace Engineering Department, California State Polytechnic University, Pomona, CA 91768 USA (e-mail: skdobbs@cpp.edu, dedberg@cpp.edu).

Analysis and Design. The investigation of [7] presents a Fuel Cell/battery Hybrid UAV.

In [8] the study investigates improving electric powered UAVS' endurance by incorporating battery dumping. Here extensions to electric powered UAVs' endurance are realized by physically dumping exhausted batteries out of the aircraft while in flight. The UAV propulsion system is considered in the study of [9], whereby simulation, design, and validation of an UAV solid oxide fuel cell (SOFC) propulsion system are presented. Trends toward the future of UAVS are studied in Small UAV Automation Using MEMS [10].

In support of UAV development, finite element based modeling studies have been used to guide the design of the UAV system. From the modeling perspective, the work of [11] details the implementation of a meta-model based correlation technique on a composite UAV wing test piece and associated finite element model. In the work of [11], MSC NASTRAN finite element models of the four structural components are correlated independently, using modal frequencies as correlation features, before being joined together into the assembled structure and compared to experimentally measured frequencies from the assembled wing in a cantilever configuration. Results show that significant improvements can be made to the assembled model fidelity.

The study of [12] presents modeling and simulation of Flexible UAVs with Large Aspect Ratio wherein the Full Non-linear equations of motion for a flexible UAV are developed. The developed model is applied to a generic UAV with large aspect ratio and the wing tip acceleration is compared to the wing tip acceleration of the rigid aircraft. The study of [13] presents results for flutter analysis of the X-HALE UAV-A test bed for aeroelastic results validation. The X-HALE UAV is a test bed exhibiting large structural deformation. Equipped with strain gauges and other measuring sensors, it will provide experimental data which can then be used for nonlinear aeroelastic analyses for other such kind of structures.

This papers deals with the linear aeroelastic analysis of this type of aircraft. The study of [14] provides open-loop flutter analysis of a composite UAV model using the active stiffening effect. From the materials and manufacturing standpoint, the work of [15] details the design and manufacture of UAV wing structure using numerical analysis of composite materials. Based on the literature review presented here, it is seen that the problem of vibrational analysis of a solar powered UAV such as the one considered in the current study is warranted.

III. Airfoil Geometry and Properties

A. Airfoil Geometry

The primary challenge with the project is the non-linear geometry of the aircraft wing. AG-25 is the airfoil profile used for the designing of the airfoil; there are 3 different sections for the wing. The first section which is attached to the fuselage is at an angel of 2° whereas the range of the airfoil scale remains constant for the section as shown in Fig. 2 from the ANSYS workbench environment.

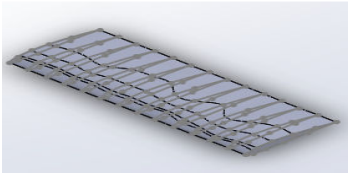

Fig. 2 First section of the left wing

The second and third sections are attached to the first and second sections at an angle of 10° and 15° with the horizontal plane respectively with the airfoil profile scale decreasing constantly till the outer tip of wing as shown in Figs. 3 and 4.

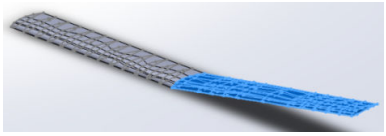

Fig. 3 Second section of the wing

Fig. 4 Third section extended at an angle of 15°

B. Material Characteristics

Mylar is one of the high performance plastic, since it is very light weight and can retain physical properties for wide temperature range it is the best option as a stressed skin for airfoil. Fig. 5 shows the linear isotropic elastic properties and physical properties of Mylar and assigning Mylar as the default material for the airfoil. Fig. 5 shows the dialog box for defining the Mylar within the ANSYS workbench suite of tools.

Properties of Outline Row 4: Mylar

	A	B	C	D	E
1	Property	Value	Unit		
2	Density	1.39	g cm^-3		
3	Isotropic Elasticity				
4	Derive from	Young's Modulus...			
5	Young's Modulus	2800	MPa		
6	Poisson's Ratio	0.37			
7	Bulk Modulus	3.5897E+09	Pa		
8	Shear Modulus	1.0219E+09	Pa		

Fig. 5 Elastic properties for Mylar

IV. Finite Element Modeling

A. Meshing

Since nonlinearities of material exist, the quality of the mesh plays a significant role since as the finer the mesh becomes, the larger does the stiffness matrix, which could potentially lead the solution to diverged solutions because of unbalanced forces. In contrast, for the coarser stiffness matrices one may encounter singular matrices for the faces which would lead to the divergence of the solution. Here, the

finite element mesh is constructed using tetrahedron cells which work well for both fluid flow systems as well as for mechanical vibrations problems. The mesh is kept at a medium quality with edge sizing for all the edges of the surface and by introducing the so-called ANSYS "sphere of influence "local mesh refinement for all of the sensitive regions of the airfoil [16]. Fig. 6 shows the meshing of the airfoil as taken from ANSYS. Since our primary objective was not to capture or analyze the vortex or downwash wake formation of the airfoil a discrete mesh size for the leading and trailing edge of the airfoil was not formulated.

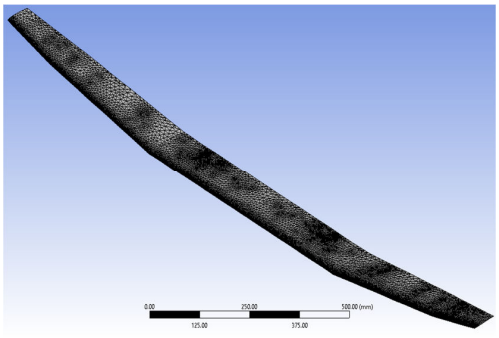

Fig. 6 Finite element mesh

V. Results and Computed Values

A. Results for Modal Analysis

Figs. 7-12 document the results for the vibration modal analysis. Fig. 7 shows the first bending mode shape for the airfoil without a lumped mass (free vibration) which shows a natural frequency in bending of 3.5004 Hz. Fig. 8 shows the first bending mode shape for the airfoil with a lumped mass at location 1 which results in a maximum frequency of 16.729 Hz. Fig. 9 gives the first bending mode shape for the airfoil with a lumped mass placed at the outer edge giving a maximum frequency of 16.616 Hz. In Fig. 9, since the mass is moved further close to the outer edge of the wing, the deformation of the wing is increased from 89.5 mm to 90 mm. For this particular project we are using subspace method for computing the eigenvalues and eigenvectors of the vibrations.

B. Results for Modal Analysis

Fig. 10 shows the second bending mode shape without lumped mass corresponding to a frequency of 17. 719 Hz. Fig. 11 shows the second bending mode shape with lumped mass at location 1 giving a frequency of 16.729 Hz. Fig. 12 indicates the second bending mode shape with the lumped mass at location 2 giving a frequency of 16.616 Hz. Fig. 13 shows the torsional modal shape for free vibrations. The maximum deformation of Fig. 13 is 99.174 mm which occurs at a frequency of 28.306 Hz. Fig. 14 shows the torsional modal shape for Airfoil with lumped mass at location 1 with maximum frequency of 26.433 Hz at the outer edge and maximum deformation of 103.1mm. Fig. 15 shows the torsional modal shape with lumped mass at spot 2 with the maximum frequency of 27.814 Hz at the outer edge and maximum deformation of 100.56 mm

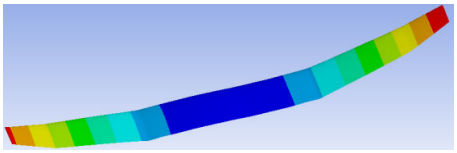

Fig. 7 Bending mode for free vibration

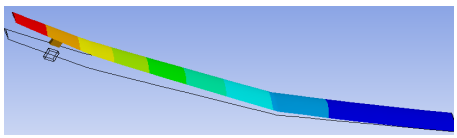

Fig. 8 1st Bending mode shape with lumped mass at location 1

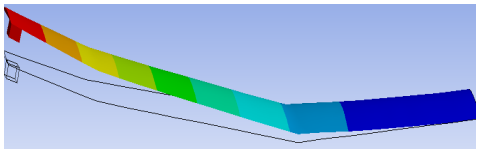

Fig. 9 Bending mode shape with lumped mass at the location 2

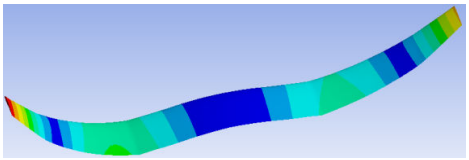

Fig. 10 2nd Bending mode shape without lumped mass

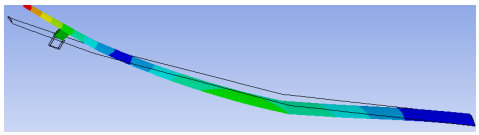

Fig. 11 2nd bending mode shape with lumped mass at spot 1

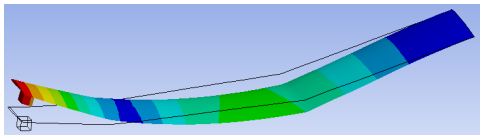

Fig. 12 2nd bending mode shape with lumped mass at location 2

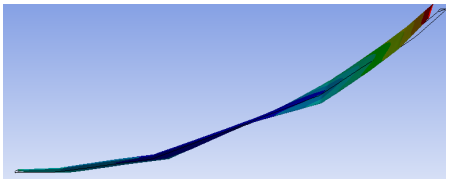

Fig. 13 Torsional mode shape for free vibrations

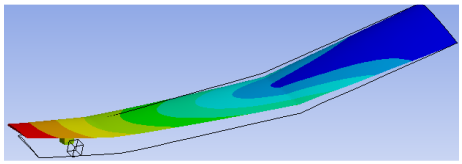

Fig. 14 Torsional Modal Shape with lumped mass at location 1

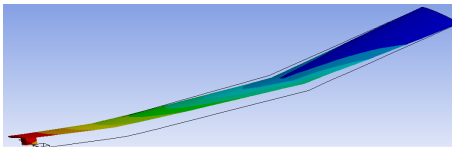

Fig. 15 Torsional Modal Shape with lumped mass at location 2

C. Fluid Structural Interaction (FSI) Analysis

The first step for the FSI setup is to figure out whether to use two way coupling or one way coupling method. In this project the more direct approach of one-way coupling was adopted in order obtain reliable and accurate results with a quick-turn-around time. By using one-way coupling the output variable of pressure is derived from ANSYS CFD FLUENT a software package and is transferred as an input parameter into Mechanical System as shown in Fig. 16 taken from ANSYS Workbench.

The work flow tree of this coupled FSI analysis within ANSYS is shown in Fig. 17. The FSI analysis was carried out by meshing a large "wind tunnel" around the airframe. This allowed the implementation of a free-stream velocity boundary condition to be input and the resulting one-way pressure coupling from the CFD package to the Mechanical Vibrations package of ANSYS to be achieved in a reasonable time fashion.

D. Result for FSI Analysis

The derived Reynolds number $Re = \rho VD/\mu$ was found to exceed Re = 500,000 so the flow is turbulent in nature. Hence the k-ε turbulence model was used to model the turbulence. The first 150 iterations were run using first order upwind followed by 850 iterations using second order upwind in order to accurately resolve the gradual change in the values for the lift coefficient C_l and drag coefficient C_d residuals. The solution converges using the first order upwind scheme at the 141st iteration and the 851st iteration for the second order upwind scheme, respectively. Using the first order upwind scheme enables the elimination of any irregularities in the values for aerodynamic forces, C_l and C_d. Fig. 18 shows the equivalent elastic stain a.k.a. von Mises Strain with the contours showing the maximum strain for the wing where it is attached to fuselage. From Fig. 18, the maximum value for von Mises strain is seen to be 0.000101 mm/mm.

Fig. 19 indicates the von Mises Stress $0.00037 < \sigma' < 0.282$ MPa with the maximum value oriented at the center of the airfoil where it engages the fuselage, as expected.

Fig. 20 shows the total deformation of the airfoil due to the aerodynamic forces ranging from $0 < w < 3.4$ mm.

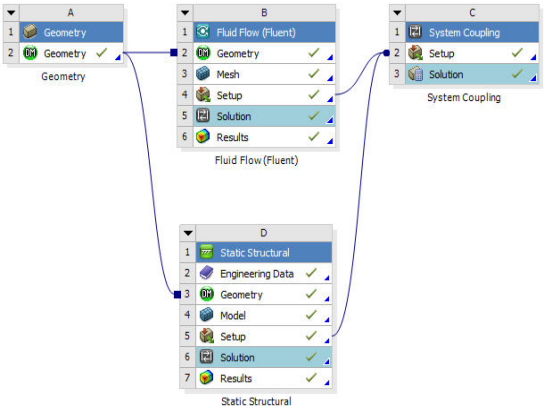

Fig. 16 FSI analysis set-up

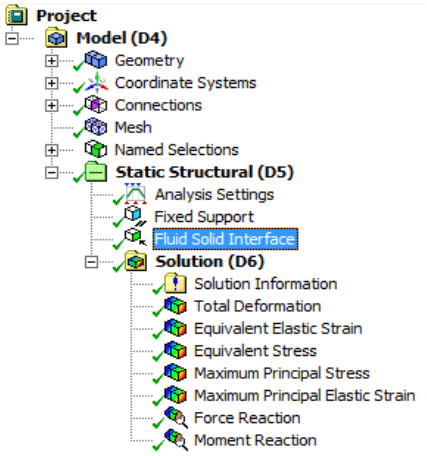

Fig. 17 Mechanical Model Outline

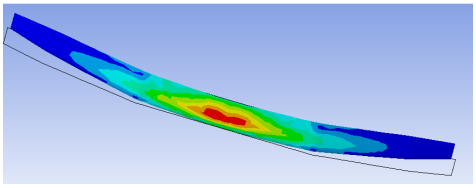

Fig. 18 Equivalent elastic stain

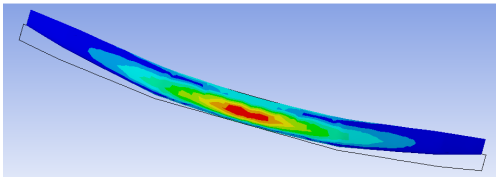

Fig. 19 von Mises Stresses

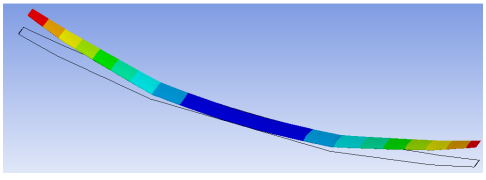

Fig. 20 Total deformation

Fig. 21 shows the dynamic pressure contours over the airfoil with pressure ranging from -1.44 kPa < p < 1.23 kPa. Fig. 22 indicates the velocity vector field over the airfoil with a magnitude ranging from 21.7 < U < 66 m/s. Fig. 23 shows the overall force reaction due to the aerodynamic forces acting on the airfoil with the reaction centered near the airfoil as expected. Fig. 24 gives the overall moment reaction for the airfoil.

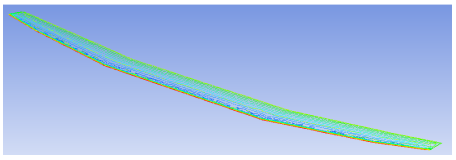

Fig. 21 Pressure contours

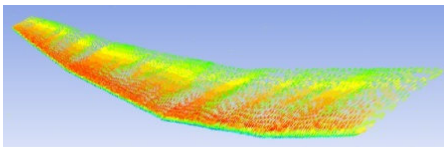

Fig. 22 Velocity vector field

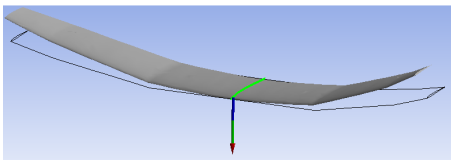

Fig. 23 Force reaction

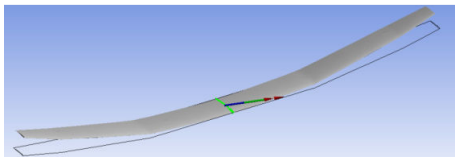

Fig. 24 Overall moment reaction

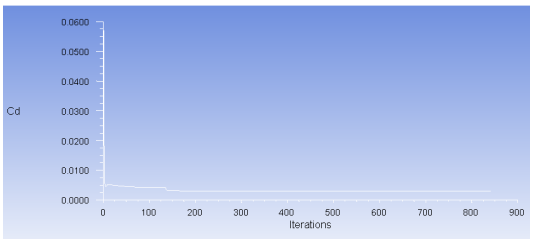

Fig. 25 Coefficient of drag

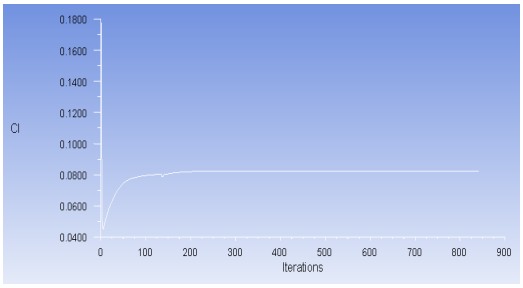

Fig. 26 Coefficient of lift

The aerodynamic derivatives of drag C_d and lift C_l are plotted in Figs. 25 and 26, respectively.

A sanity check was performed on the coefficient of drag and coefficient of lift by performing back-of-the-envelope calculations. These hand-calculated values of of C_d=0.005167, and C_l=0.07698 shown in Table I together with other miscellaneous aerodynamic force parameters. The hand compute values of Table I are found to be in reasonable agreement with the numerical FSI results as shown the asymptotes of Figs. 25 and 26, respectively.

TABLE I
AERODYNAMIC FORCE RESULTS

	Parameter	Value
C_l	Lift coefficient	0.077
C_d	Drag coefficient	0.0052
C_l/C_d	Lift/drag ratio	14.9
D	Drag force	11.74
L	Lift Force	47.83
CP	Center of pressure	(x,y,z) = (-6.8, -10.09,1.669)
M	Pressure moment	-50.96 in +X-dir.
C	Pressure coefficient	-3.1 < C < 0.98

VI. CONCLUSIONS

This paper has presented the results of a Finite Element based vibration analysis of a solar powered Unmanned Aerial Vehicle (UAV). The motivation of this study was to aid in the design and development of a solar powered UAV which was constructed by Cal Poly Pomona's Aerospace Engineering Department. The solar battery powered UAV uses vibration induced magnet-in-coil power generators embedded in its airfoil and excited by gusts and control surface pulse-decays to augment the power required for the electric motor flight. Using FEM based Vibration Analysis affords the design team a better indication of where to locate these actuators. FEM was used to mimic the location of the actuators as a point load (or stinger) in the vibrational modal analysis. Results show that the free mode in bending is 4.8 Hz while, depending on the location of excitation (either at the wing tip or slightly inward of the wing tip), the first forced bending mode is on range of 16.2 to 16.7 Hz. Thus, the forced bending mode is seen to be far from the free bending mode, but the range of the forced bending mode is small. The free torsional bending mode is 28.3 Hz, and again depending on the location of excitation, the first forced torsional mode ranges from 26.4 to 27.8 Hz. Thus

the first torsional mode is seen to be very close to the torsional natural frequency for two different excitation locations. The FSI results predict the aerodynamic drag and lift of Cd = 0.0052 and C_l = 0.077 respectively, affording a lift/drag ratio of C_l/C_d = 14.9. Hand-calculations used to validate the finite element results. The FSI results give a maximum von Mises of 0.282 and a maximum airfoil deflection of 3.4 mm. Dynamic pressures on the airfoil ranges from 1.04 to 1.23 kPa corresponding to velocity magnitudes of 22 to 66 m/s. Future work will entail the flutter analysis of the rear tail rudder of the UAV.

REFERENCES

[1] Lee, Bohwa, Poomin Park, Keunbae Kim, and Sejin Kwon. 2014. The Flight Test and Power Simulations of an UAV Powered by Solar Cells, a Fuel Cell and Batteries. *Journal of Mechanical Science and Technology*. 28, no. 1: 399-405.

[2] 2008. Solar-powered UAV Takes Flight. *Reinforced Plastics*. 52, no. 9: 5.

[3] Anonymous. 2005. Solar-powered UAV Flies Two Days Straight. *Machine Design*. 77, no. 16: 26.

[4] Jashnani, S, T.R Nada, M Ishfaq, A Khamker, and P Shaholia. 2013. Sizing and Preliminary Hardware Testing of Solar Powered UAV. *The Egyptian Journal of Remote Sensing and Space Science*.

[5] 2007. Custom Battery Pack Powers UAV. *Power Electronics Technology (Online Exclusive)*.

[6] Suzuki, Koji, Paulo Kemper Filho, and James Morrison. 2012. Automatic Battery Replacement System for UAVs: Analysis and Design. *Journal of Intelligent & Robotic Systems*. 65, no. 1: 563-586.

[7] 2010. Fuel Cell/battery Hybrid UAV Takes off in Taiwan. *Fuel Cells Bulletin*. 2010, no. 6: 4-5.

[8] Chang, Tan, and Hu Yu. 2015. Improving Electric Powered UAVs' Endurance by Incorporating Battery Dumping Concept. *Procedia Engineering*. 99: 168-179.

[9] Lindahl, P, E Moog, and S. R Shaw. 2012. Simulation, Design, and Validation of an UAV SOFC Propulsion System. *IEEE Transactions on Aerospace and Electronic Systems*. 48, no. 3: 2582-2593.

[10] Jang, Jung Soon, and D Liccardo. 2007. Small UAV Automation Using MEMS. *IEEE Aerospace and Electronic Systems Magazine*. 22, no. 5: 30-34.

[11] Oliver, Joseph A, John B Kosmatka, François M Hemez, and Charles R Farrar. 2007. Finite Element Model Correlation of a Composite UAV Wing Using Modal Frequencies. *Proceedings of SPIE*. 6532, no. 1.

[12] Haghighat, Sohrab, S Haghighat, Hugh H.T Liu, H.H.T Liu, J.R.R.A Martins, and Joaquim R.R.A Martins. 2008. Modeling and Simulation of Flexible UAVs with Large Aspect Ratio. *2008 Asia Simulation Conference - 7th International Conference on System Simulation and Scientific Computing*. 504-509.

[13] Ahmad, Kamran, and Hammad Rahman. 2012. Flutter Analysis of X-HALE UAV-A Test Bed for Aeroelastic Results Validation. *Applied Mechanics and Materials*. 245: 303.

[14] Waisman, H. 2004. Open-loop Flutter Analysis of a Composite UAV Model Using the Active Stiffening Effect. *Finite Elements in Analysis and Design*. 40, no. 11: 1283-1295.

[15] Grodzki, W, and A Łukaszewicz. 2015. Design and Manufacture of Unmanned Aerial Vehicles (UAV) Wing Structure Using Composite Materials.*Materialwissenschaft Und Werkstofftechnik*. 46, no. 3: 269-278

[16] 2009. Best Practice Guidelines for handling Automotive External Aerodynamics with Fluent. *Marco Lanfrit.* : 3-4

Kevin R. Anderson obtained his BSME in Mechanical Engineering at Cal Poly Pomona in 1991, MSME in Mechanical Engineering at the University of Colorado at Boulder, and Ph.D. in Mechanical Engineering at the University of Colorado at Boulder in 1998. He holds a PE license and over 15 years of practical engineering experience. He is currently a Professor of Mechanical Engineering and Director of the Non-linear FEM/CFD Multiphysics Simulation Lab at California State Polytechnic University, Pomona (Cal Poly Pomona). He has a variety of publications in Machine Design, Vibration Flutter Analysis, Computational Fluid Dynamics (CFD), and Control Systems.

Sukhwinder Singh obtained his BSME in 2014 at Chandigarh College of Engineering and Technology, Punjab University. He is currently a Master's Student in Mechanical Engineering at Cal Poly Pomona.

Nouh Aines obtained his BSc in Electromechanical Engineering in 2012 at Alexandria University, Alexandria, Egypt. He is currently a Master's Student in Mechanical Engineering at Cal Poly Pomona.

Shilpa Ravichandra obtained her BSAE in 2011 at Jawaharlal Nehru Technological University, Hyderabad, India. She is currently a Master's Student in Mechanical Engineering at Cal Poly Pomona.

Steven Dobbs obtained his BS in Aerospace Engineering at Cal Poly Pomona in 1970, his MS in Mechanical Engineering at Cal State Long Beach in 1979. He possesses over thirty years of practical experience in the field of Aerospace Systems Engineering and Aeroelastic Analysis. He is currently a Professional Practice Professor in Aerospace Engineering at Cal Poly Pomona.

Donald Edberg obtained his BS in Applied Mechanics and Engineering Sciences from UCSD in 1978, his Aeronautical and Astronautical Engineering from Stanford in 1970 and his PhD in Aeronautical and Astronautical Engineering from Stanford in 1984. He possesses over twenty years of practical experience in the field of Aerospace Structural Dynamics and Control. He is currently Director of the Astronautics Laboratory in Aerospace Engineering at Cal Poly Pomona.